macrophage markers, *Arg1*, *Fizz1*, and *Ym1*, were significantly elevated in *Fli1*$^{+/-}$ mice compared with WT mice at day 7 (Figure 6A), while comparable at baseline (Figure S3). Consistently, the number of arginase 1-positive macrophages in the lesional skin was significantly increased in *Fli1*$^{+/-}$ mice compared with WT mice at day 7 (Figure 6B). In addition, IL-4 and IL-13 induced polarization of macrophages towards the M2 phenotype to a greater extent in peritoneal macrophages isolated from *Fli1*$^{+/-}$ mice than in those from WT mice (Figure 6C). Collectively, these results indicate that Fli1 haploinsufficiency promotes M2 macrophage infiltration in the lesional skin of BLM-treated mice by inducing M2 differentiation of macrophages via an intrinsic mechanism triggered by BLM.

Discussion

In this study, we demonstrate that Fli1 haploinsufficiency exacerbates BLM-induced dermal fibrosis through multiple mechanisms, including induction of an SSc-like phenotype in dermal fibroblasts, endothelial cell and macrophages, the Th2/Th17 polarized inflammation and increased mast cell infiltration. These results support the concept of the multifactorial nature of SSc and place Fli1 deficiency as a predisposing factor of this disease.

Fli1 is a potent repressor of the *COL1A1* and *COL1A2* genes and its downregulation is a critical step to induce matrix gene expression in dermal fibroblasts (4, 6-10). In the skin of *Fli1*$^{+/-}$ mice, mRNA levels of the *Col1a2* gene were markedly increased and the levels of soluble type I collagen were also elevated (Figure S6), indicating that Fli1 haploinsufficiency activates dermal fibroblasts *in vivo*. However, dermal thickness was comparable between *Fli1*$^{+/-}$ and WT mice. While counterintuitive, this observation is plausible because there was no difference between *Fli1*$^{+/-}$ and WT mice in CTGF expression, which is indispensable to establish and maintain dermal fibrosis *in vivo* (28, 45, 46). Supporting this, BLM increased CTGF expression as well

as dermal thickness to a greater extent in *Fli1*$^{+/-}$ mice than in WT mice. Although the detailed mechanism underlying the BLM-dependent CTGF induction in *Fli1*$^{+/-}$ dermal fibroblasts is not fully elucidated, up-regulated expression of αVβ3 and αVβ5 integrins and activation of latent TGF-β may contribute to the enhanced expression of pro-fibrotic genes, including CTGF. Indeed, it was recently reported that the αV-containing integrins collectively regulate the key pro-fibrotic pathways during organ fibrosis (47).

Aberrant vascular activaiton plays a central role together with inflammation and autoimmunity in initiation and maintenance of tissue fibrosis in SSc. Since *Fli1* ECKO mice reproduce the histological abnormalities and increased vascular permeability characteristic of SSc, Fli1 deficiency is also a potential predisposing factor of SSc vascular activation. To explore if Fli1 deficiency links vascular event to tissue fibrosis in SSc, we evaluated the impact of Fli1 haploinsufficiency on cell adhesion molecules regulating Th2/Th17 skewed inflammation and on EndoMT. The pro-fibrotic cell adhesion molecules, ICAM1 and GlyCAM1, were increased while the anti-fibrotic cell adhesion molecules, P-selectin and E-selectin, were decreased in BLM-treated *Fli1*$^{+/-}$ mice, which theoretically promotes Th2/Th17 skewed immune polarization. Consistently, the expression levels of the *Il4*, *Il6*, *Il10* and *Il17a* genes were elevated while those of the *Il12a* gene were decreased in BLM-treated *Fli1*$^{+/-}$ mice at 7 days. Given that immune polarization in diffuse cutaneous SSc generally shifts from Th2/Th17 to Th1 in parallel with disease duration and that mRNA levels of the *ICAM1* and *GlyCAM1* genes are relatively higher than those of the *SELP* and *SELE* genes in the skin of early diffuse cutaneous SSc (Figure S7), the altered expression of cell adhesion molecules in endothelial cells due to Fli1 deficiency may contribute to the induction of inflammatory cell infiltration characteristic of SSc. Furthermore, in contrast to PBS-treated WT mice, EndoMT was observed in PBS-treated *Fli1*$^{+/-}$ mice and was induced to a greater extent in BLM-treated *Fli1*$^{+/-}$ mice than in BLM-treated WT mice.

Importantly, key molecules regulating EndoMT, including VE-cadherin, FSP1 and Snail-1, were shown to be the direct targets of Fli1. Collectively, Fli1 deficiency potentially promotes the induction of a pro-fibrotic phenotype in dermal microvascular endothelial cells especially in the presence of certain environmental influences in SSc.

The monocyte-macrophage lineages are characterized by considerable diversity and plasticity, which is regulated by a complicated network of signaling molecules, transcription factors, and epigenetic mechanisms. The present study demonstrates that Fli1 haploinsufficiency promotes the expansion of M2 macrophages in the lesional skin of BLM-treated mice and M2 differentiation of peritoneal macrophages in response to IL-4 or IL-13 stimulation *in vitro*, suggesting that Fli1 haploinsufficiency could directly contribute to the differentiation of M2 macrophages. Given that M2 macrophages represent the predominant macrophage subset in the lesional skin of early diffuse cutaneous SSc (39), Fli1 haploinsufficiency may also serve as a predisposing factor to induce the SSc phenotype in response to environmental influences in macrophages.

Another important observation in this study was that Fli1 haploinsufficiency increased mast cell infiltration and the $CD4^+/CD8^+$ ratio of infiltrating lymphocytes upon BLM treatment in the lesional skin. In SSc patients evidence has demonstrated that mast cells are increased and serve as a major producer of TGF-β in the lesional skin and that the $CD4^+/CD8^+$ ratio is increased in the peripheral blood and the lesional skin (38, 48). Although the detailed mechanism regulating mast cell infiltration and the significance of the elevated $CD4^+/CD8^+$ ratio are not well understood, the present observation further supports the idea that Fli1 deficiency is also a predisposing factor integrating the induction of the SSc phenotype in various inflammatory cells.

In summary, this study provides strong evidence for the fundamental role of Fli1 deficiency in inducing SSc-like phenotypic alterations in dermal fibroblasts, endothelial cells, and macrophages in a manner consistent with human disease. These results support the canonical idea that epigenetic reprogramming underlies pathogenic

changes in SSc and implicate the Fli1 deficiency-dependent pathway as a central mediator of this disease.

References

1. Asano Y. Future treatments in systemic sclerosis. J Dermatol. 2010;37:54-70.

2. Asano Y, Sato S. Animal models of scleroderma: current state and recent development. Curr Rheumatol Rep. 2013;15:382.

3. Wang Y, Fan PS, Kahaleh B. Association between enhanced type I collagen expression and epigenetic repression of the FLI1 gene in scleroderma fibroblasts. Arthritis Rheum. 2006;54:2271-9.

4. Asano Y, Czuwara J, Trojanowska M. Transforming growth factor-β regulates DNA binding activity of transcription factor Fli1 by p300/CREB-binding protein-associated factor-dependent acetylation. J Biol Chem. 2007;282:34672-83.

5. Chrobak I, Lenna S, Stawski L, Trojanowska M. Interferon-γ promotes vascular remodeling in human microvascular endothelial cells by upregulating endothelin (ET)-1 and transforming growth factor (TGF) β2. J Cell Physiol. 2013;228:1774-83.

6. Asano Y, Trojanowska M. Phosphorylation of Fli1 at threonine 312 by protein kinase C δ promotes its interaction with p300/CREB-binding protein-associated factor and subsequent acetylation in response to transforming growth factor β. Mol Cell Biol. 2009;29:1882-94.

7. Kubo M, Czuwara-Ladykowska J, Moussa O, Markiewicz M, Smith E, Silver RM, et al. Persistent down-regulation of Fli1, a suppressor of collagen transcription, in fibrotic scleroderma skin. Am J Pathol. 2003;163:571-81.

8. Asano Y, Markiewicz M, Kubo M, Szalai G, Watson DK, Trojanowska M. Transcription factor Fli1 regulates collagen fibrillogenesis in mouse skin. Mol Cell Biol. 2009;29:425-34.

9. Czuwara-Ladykowska J, Shirasaki F, Jackers P, Watson DK, Trojanowska M. Fli-1 inhibits collagen type I production in dermal fibroblasts via an Sp1-dependent pathway. J Biol Chem. 2001;276:20839-48.

10. Nakerakanti SS, Kapanadze B, Yamasaki M, Markiewicz M, Trojanowska M. Fli1 and Ets1 have distinct roles in connective tissue growth factor/CCN2 gene regulation and induction of the profibrotic gene program. J Biol Chem. 2006;281:25259-69.

11. Noda S, Asano Y, Akamata K, Aozasa N, Taniguchi T, Takahashi T, et al. A possible contribution of altered cathepsin B expression to the development of skin sclerosis and vasculopathy in systemic sclerosis. PLoS One. 2012;7:e32272.

12. Noda S, Asano Y, Takahashi T, Akamata K, Aozasa N, Taniguchi T, et al. Decreased cathepsin V expression due to Fli1 deficiency contributes to the development of dermal fibrosis and proliferative vasculopathy in systemic sclerosis. Rheumatology (Oxford). 2013;52:790-9.

13. Chan ES, Liu H, Fernandez P, Luna A, Perez-Aso M, Bujor AM, et al. Adenosine A2A receptors promote collagen production by a Fli1- and CTGF-mediated mechanism. Arthritis Res Ther. 2013;15:R58.

14. Bujor AM, Haines P, Padilla C, Christmann RB, Junie M, Sampaio-Barros PD, et al. Ciprofloxacin has antifibrotic effects in scleroderma fibroblasts via downregulation of Dnmt1 and upregulation of Fli1. Int J Mol Med. 2012;30:1473-80.

15. Nakerakanti SS, Bujor AM, Trojanowska M. CCN2 is required for the TGF-β induced activation of Smad1-Erk1/2 signaling network. PLoS One. 2011;6:e21911.

16. Asano Y, Stawski L, Hant F, Highland K, Silver R, Szalai G, et al. Endothelial Fli1 deficiency impairs vascular homeostasis: a role in scleroderma vasculopathy. Am J Pathol. 2010;176:1983-98.

17. Spyropoulos DD, Pharr PN, Lavenburg KR, Jackers P, Papas TS, Ogawa M, et al. Hemorrhage, impaired hematopoiesis, and lethality in mouse embryos carrying a targeted disruption of the Fli1 transcription factor. Mol Cell Biol. 2000;20:5643-52.

18. Yamamoto T, Takagawa S, Katayama I, Yamazaki K, Hamazaki Y, Shinkai H, et al. Animal model of sclerotic skin. I: Local injections of bleomycin induce sclerotic

skin mimicking scleroderma. J Invest Dermatol. 1999;112:456-62.

19. Yoshizaki A, Iwata Y, Komura K, Ogawa F, Hara T, Muroi E, et al. CD19 regulates skin and lung fibrosis via Toll-like receptor signaling in a model of bleomycin-induced scleroderma. Am J Pathol. 2008;172:1650-63.

20. Asano Y, Ihn H, Yamane K, Kubo M, Tamaki K. Impaired Smad7-Smurf-mediated negative regulation of TGF-β signaling in scleroderma fibroblasts. J Clin Invest. 2004;113:253-64.

21. Zeini M, Través PG, López-Fontal R, Pantoja C, Matheu A, Serrano M, et al. Specific contribution of p19(ARF) to nitric oxide-dependent apoptosis. J Immunol. 2006;177:3327-36.

22. Asano Y, Ihn H, Yamane K, Jinnin M, Tamaki K. Increased expression of integrin αVβ5 induces the myofibroblastic differentiation of dermal fibroblasts. Am J Pathol. 2006;168:499-510.

23. Miller EJ, Rhodes RK. Preparation and characterization of the different types of collagen. Methods Enzymol. 1982;82 Pt A:33-64.

24. Markiewicz M, Asano Y, Znoyko S, Gong Y, Watson DK, Trojanowska M. Distinct effects of gonadectomy in male and female mice on collagen fibrillogenesis in the skin. J Dermatol Sci. 2007;47:217-26.

25. Yamamoto T, Takahashi Y, Takagawa S, Katayama I, Nishioka K. Animal model of sclerotic skin. II. Bleomycin induced scleroderma in genetically mast cell deficient WBB6F1-W/W(V) mice. J Rheumatol. 1999;26:2628-34.

26. Yamamoto T, Kuroda M, Nishioka K. Animal model of sclerotic skin. III: Histopathological comparison of bleomycin-induced scleroderma in various mice strains. Arch Dermatol Res. 2000;292:535-41.

27. Takagawa S, Lakos G, Mori Y, Yamamoto T, Nishioka K, Varga J. Sustained activation of fibroblast transforming growth factor-β/Smad signaling in a murine model of scleroderma. J Invest Dermatol. 2003;121:41-50.

28. Mori T, Kawara S, Shinozaki M, Hayashi N, Kakinuma T, Igarashi A, et al. Role and interaction of connective tissue growth factor with transforming growth factor-β in persistent fibrosis: A mouse fibrosis model. J Cell Physiol. 1999;181:153-9.

29. Asano Y, Ihn H, Yamane K, Kubo M, Tamaki K. Increased expression levels of integrin αVβ5 on scleroderma fibroblasts. Am J Pathol. 2004;164:1275-92.

30. Asano Y, Ihn H, Yamane K, Jinnin M, Mimura Y, Tamaki K. Increased expression of integrin αVβ3 contributes to the establishment of autocrine TGF-β signaling in scleroderma fibroblasts. J Immunol. 2005;175:7708-18.

31. Asano Y, Ihn H, Yamane K, Jinnin M, Mimura Y, Tamaki K. Involvement of αVβ5 integrin-mediated activation of latent transforming growth factor β1 in autocrine transforming growth factor β signaling in systemic sclerosis fibroblasts. Arthritis Rheum. 2005;52:2897-905.

32. Abe M, Harpel JG, Metz CN, Nunes I, Loskutoff DJ, Rifkin DB. An assay for transforming growth factor-β using cells transfected with a plasminogen activator inhibitor-1 promoter-luciferase construct. Anal Biochem. 1994;216:276-84.

33. Kizu A, Medici D, Kalluri R. Endothelial-mesenchymal transition as a novel mechanism for generating myofibroblasts during diabetic nephropathy. Am J Pathol. 2009;175:1371-3.

34. Zeisberg EM, Tarnavski O, Zeisberg M, Dorfman AL, McMullen JR, Gustafsson E, et al. Endothelial-to-mesenchymal transition contributes to cardiac fibrosis. Nat Med. 2007;13:952-61.

35. Li J, Qu X, Bertram JF. Endothelial-myofibroblast transition contributes to the early development of diabetic renal interstitial fibrosis in streptozotocin-induced diabetic mice. Am J Pathol. 2009;175:1380-8.

36. Hashimoto N, Phan SH, Imaizumi K, Matsuo M, Nakashima H, Kawabe T, et al. Endothelial-mesenchymal transition in bleomycin-induced pulmonary fibrosis. Am J Respir Cell Mol Biol. 2010;43:161-72.

37. Yoshizaki A, Yanaba K, Iwata Y, Komura K, Ogawa A, Akiyama Y, et al. Cell adhesion molecules regulate fibrotic process via Th1/Th2/Th17 cell balance in a bleomycin-induced scleroderma model. J Immunol. 2010;185:2502-15.

38. Hussein MR, Hassan HI, Hofny ER, Elkholy M, Fatehy NA, Abd Elmoniem AE, et al. Alterations of mononuclear inflammatory cells, CD4/CD8+ T cells, interleukin 1β, and tumour necrosis factor α in the bronchoalveolar lavage fluid, peripheral blood, and skin of patients with systemic sclerosis. J Clin Pathol. 2005;58:178-84.

39. Higashi-Kuwata N, Jinnin M, Makino T, Fukushima S, Inoue Y, Muchemwa FC, et al. Characterization of monocyte/macrophage subsets in the skin and peripheral blood derived from patients with systemic sclerosis. Arthritis Res Ther. 2010;12:R128.

40. Ploeger DT, Hosper NA, Schipper M, Koerts JA, de Rond S, Bank RA. Cell plasticity in wound healing: paracrine factors of M1/ M2 polarized macrophages influence the phenotypical state of dermal fibroblasts. Cell Commun Signal. 2013;11:29.

41. Han Y, Ma FY, Tesch GH, Manthey CL, Nikolic-Paterson DJ. Role of macrophages in the fibrotic phase of rat crescentic glomerulonephritis. Am J Physiol Renal Physiol. 2013;304:F1043-53.

42. Wang J, Jiang ZP, Su N, Fan JJ, Ruan YP, Peng WX, et al. The role of peritoneal alternatively activated macrophages in the process of peritoneal fibrosis related to peritoneal dialysis. Int J Mol Sci. 2013;14:10369-82.

43. Hamilton RF, Parsley E, Holian A. Alveolar macrophages from systemic sclerosis patients: evidence for IL-4-mediated phenotype changes. Am J Physiol Lung Cell Mol Physiol. 2004;286:L1202-9.

44. Mathai SK, Gulati M, Peng X, Russell TR, Shaw AC, Rubinowitz AN, et al. Circulating monocytes from systemic sclerosis patients with interstitial lung disease show an enhanced profibrotic phenotype. Lab Invest. 2010;90:812-23.

45. Liu S, Shi-wen X, Abraham DJ, Leask A. CCN2 is required for bleomycin-induced skin fibrosis in mice. Arthritis Rheum. 2011;63:239-46.

46. Liu S, Parapuram SK, Leask A. Fibrosis caused by loss of PTEN expression in mouse fibroblasts is crucially dependent on CCN2. Arthritis Rheum. 2013;65:2940-4.

47. Henderson NC, Arnold TD, Katamura Y, Giacomini MM, Rodriguez JD, McCarty JH, et al. Targeting of αV integrin identifies a core molecular pathway that regulates fibrosis in several organs. Nat Med. 2013;19:1617-24.

48. Hügle T, Hogan V, White KE, van Laar JM. Mast cells are a source of transforming growth factor β in systemic sclerosis. Arthritis Rheum. 2011;63:795-9.

Figure legends

Figure 1. Fli1 haploinsufficiency exacerbates BLM-induced dermal fibrosis.

A, B. Representative skin sections of both WT and *Fli1*$^{+/-}$ mice at day 28 after PBS or BLM injection (A: hematoxylin and eosin staining, B: Masson's trichrome staining). Vertical arrows indicate the dermal thickness. Dermal thickness and collagen content measured by hydroxyproline assay of each group are summarized in the right panels of A and B, respectively (n = 4-8). Relative ratio of each group is shown with PBS-treated WT mice set at 1. **C.** The relative number of myofibroblasts in the dermis. The number per high-power field is adjusted to that in PBS-treated WT mice set at 1 (n = 4-5). The representative pictures of skin histology in WT and *Fli1*$^{+/-}$ mice treated with PBS or BLM are shown in the left panels. Insets depict fibroblasts with higher magnification. Detailed data were shown in Table S3. Values are the means ± SEM. *P <0.05, **P <0.01, ***P <0.001. Bars, 50 μm.

Figure 2. Fli1 haploinsufficiency amplifies BLM-induced expression of CTGF, integrin αVβ3 and αVβ5 in dermal fibroblasts.

A. mRNA expression of the *Tgb1*, *Ctgf*, *Itgav*, *Itgb3*, and *Itgb5* genes in the skin tissue at day 28 after PBS or BLM injection (n = 10). **B.** mRNA expression of the *ITGAV*, *ITGB3*, and *ITGB5* genes in SCR or Fli1 siRNA-transfected dermal fibroblasts treated with TGF-β1 or not (n = 6). **C.** The luciferase activities of TMLC co-cultured in the presence or absence of cell-cell contact with SCR or Fli1 siRNA-transfected dermal fibroblasts treated with TGF-β1 or not (n= 4-6; left and middle panels) and the luciferase activities of TMLC co-cultured in the presence of RGD or RGE peptides with SCR or Fli1 siRNA-transfected dermal fibroblasts treated with TGF-β1 or not (n = 6; a right panel). **D.** mRNA expression of the *CTGF* gene in SCR or Fli1 siRNA-transfected dermal fibroblasts treated with TGF-β1 or not (n = 4; a left panel) and in SCR or Fli1

siRNA-transfected dermal fibroblasts treated with TGF-β1 in the presence of RGD or RGE peptides (n= 3; a right panel). Detailed data were shown in Table S4. Values are the means ± SEM. *P <0.05, **P <0.01, ***P <0.001. NS, not significant. AU, arbitrary unit.

Figure 3. EndoMT is directly induced by Fli1 haplosufficiency and further facilitated by BLM.

A. Immunofluorescence staining for FSP1 (green) and VE-cadherin (red) in skin samples from each group. FSP1/VE-cadherin double positive cells were indicated by arrows. Insets depict representative cells with higher magnification (double positive cells for BLM-treated WT mice and PBS- and BLM-treated *Fli1*$^{+/-}$ mice and a FSP1 single positive cell for PBS-treated WT mice). **B.** The number of FSP1/VE-cadherin double positive cells was counted under magnification x 200 (n = 4). **C.** mRNA expression of the *VE-cadherin*, *ACTA2*, *FSP1*, and *SNAI1* genes in HDMECs transfected with SCR or Fli1 siRNA (n = 6). **D.** Chromatin immunoprecipitation analysis of Fli1 binding to the promoters of the *FSP1* and *SNAI1* genes. Detailed data were shown in Table S5. Values are the means ± SEM. *P <0.05. AU, arbitrary unit. Bar, 20 μm.

Figure 4. Fli1 haploinsufficiency modulates the expression of cell adhesion molecules in dermal microvascular endothelial cells leading to the induction of Th2/17 skewed inflammation.

A. mRNA levels of the *Icam1*, *Glycam1*, *Selp* and *Sele* genes in the skin of WT and *Fli1*$^{+/-}$ mice treated with BLM for 7 days (n = 10). **B.** mRNA expression of the *ICAM1*, *GlyCAM1*, *SELP*, and *SELE* genes in HDMECs transfected with SCR or Fli1 siRNA (n = 6). **C.** Chromatin immunoprecipitation analysis of Fli1 binding to the promoters of the *ICAM1*, *SELP*, and *SELE* genes. Detailed data were shown in Table S6. Values are the

means ± SEM. *P <0.05. AU, arbitrary unit.

Figure 5. Fli1 haploinsufficiency induces the expression profiles of cytokines and chemokines characteristic of SSc and promotes an SSc-like inflammatory infiltration in BLM-treated mice.

A. mRNA levels of the *Il1b*, *Il4*, *Il6*, *Il10*, *Il12a*, *Il17a*, *Ifng*, *Tnfa*, and *Mcp1* genes in the skin of WT and *Fli1*$^{+/-}$ mice at day 7 after BLM injection (n = 10). **B.** The number of CD4^{+} T cells, CD8^{+} T cells, mast cells, and macrophages in the lesional skin of PBS- and BLM-treated WT mice and *Fli1*$^{+/-}$ mice at day 7 and 28 (n = 5). **C.** The ratio of CD4^{+}/CD8^{+} T cells in the lesional skin of PBS and BLM-treated WT mice and *Fli1*$^{+/-}$ mice at day 7 and 28 (n = 5; *P <0.05). Cells were counted in 10 random grids under magnification of x 400 high-power fields. Representative images are shown in Figure S5. Detailed data were shown in Table S7. Values are the means ± SEM. ; *P <0.05. HPF, high-power field. AU, arbitrary unit.

Figure 6. Fli1 haploinsufficiency promotes M2 macrophages infiltration in the skin of BLM-treated mice and M2 differentiation of peritoneal macrophages by IL-4 or IL-13 stimulation.

A. mRNA levels of the *Arg1*, *Fizz1*, and *Ym1* genes in the skin of WT and *Fli1*$^{+/-}$ mice at day 7 after BLM injection (n = 10). **B.** The number of arginase 1-positive macrophages in the skin of WT and *Fli1*$^{+/-}$ mice at day 7 and 28 after PBS or BLM injection (n = 5). **C.** mRNA levels of the *Arg1*, *Fizz1*, and *Ym1* genes in peritoneal macrophages from WT and *Fli1*$^{+/-}$ mice treated with IL-4 or IL-13 (n = 4). Detailed data were shown in Table S8. Values are the means ± SEM. *P <0.05, **P <0.01. AU, arbitrary unit.

Figure S1. Immunostaining for CTGF in skin samples from PBS or BLM treated WT or *Fli1*$^{+/-}$ mice.

A. The representative pictures of immunostaining for CTGF in skin samples from WT and *Fli1*$^{+/-}$ mice treated with PBS or BLM. **B.** The relative number of CTGF-positive fibroblasts and FSP1/CTGF double positive fibroblasts in the dermis. The number per high-power field is adjusted to that in PBS-treated WT mice set at 1 (n = 5). **C.** The representative pictures of immunofluorescence for FSP1 (green) and CTGF (red) in skin samples from WT and *Fli1*$^{+/-}$ mice treated with PBS or BLM. Double positive cells were indicated by arrows. Values are the means ± SEM. *P < 0.05. Bars, 10 μm.

Figure S2. Immunostaining for integrin β3 in skin samples from PBS or BLM treated WT or *Fli1*$^{+/-}$ mice.

A. The representative pictures of immunostaining for integrin β3 in skin samples from WT and *Fli1*$^{+/-}$ mice treated with PBS or BLM. **B.** The relative number of FSP1/integrin β3 double positive fibroblasts in the dermis. The number per high-power field is adjusted to that in PBS-treated WT mice set at 1 (n = 5). **C.** The representative pictures of immunofluorescence for FSP1 (green) and integrin β3 (red) in skin samples from WT and *Fli1*$^{+/-}$ mice treated with PBS or BLM. Double positive cells were indicated by arrows. Values are the means ± SEM. *P < 0.05. Bars, 10 μm.

Figure S3. Immunostaining for integrin β5 in skin samples from PBS or BLM treated WT or *Fli1*$^{+/-}$ mice.

A. The representative pictures of immunostaining for integrin β5 in skin samples from WT and *Fli1*$^{+/-}$ mice treated with PBS or BLM. **B.** The relative number of FSP1/integrin β5 double positive fibroblasts in the dermis. The number per high-power field is adjusted to that in PBS-treated WT mice set at 1 (n = 5). **C.** The representative pictures of immunofluorescence for FSP1 (green) and integrin β5 (red) in skin samples from WT and *Fli1*$^{+/-}$ mice treated with PBS or BLM. Double positive cells were indicated by arrows. Values are the means ± SEM. *P < 0.05. Bars, 10 μm.

Figure S4. The expression profiles of cytokines, chemokines, and M2 macrophage markers in the lesional skin of PBS-treated mice.

mRNA levels of the *Il1b, Il4, Il6, Il10, Il12a, Il17a, Ifng, Tnfa, Mcp1, Arg1, Fizz1,* and *Ym1* genes were measured in the skin of WT and *Fli1*$^{+/-}$ mice with PBS treatment. Values are the means ± SEM (n = 4-8). ND; not determined. AU, arbitrary unit.

Figure S5. The evaluation of inflammatory cell infiltration in mice treated with PBS or BLM.

The representative pictures of F4/80, toluidine blue, CD4, and CD8 staining are shown in the skin of WT and *Fli1*$^{+/-}$ mice at day 7 and 28 after PBS or BLM injection (n = 5).

Figure S6. mRNA levels of the *Col1a2* gene and the levels of soluble type I collagen in the skin of WT and *Fli1*$^{+/-}$ mice.

A. mRNA expression of the *Col1a2* gene in the skin tissue of WT and *Fli1*$^{+/-}$ mice at day 28 after PBS injection were assessed (n = 10). **B.** The levels of soluble type I collagen were elevated in *Fli1*$^{+/-}$ mice. Pepsin-soluble collagen was stained with Coomassie blue (a left panel). Arrows indicate collagen α1(I) and α2(I) subunits. β-components represent cross-linked α-chain dimers. Collagen levels were quantitated using public domain software ImageJ (n = 3; a right panel). Values are the means ± SEM. *$P < 0.05$, ***$P < 0.001$. AU, arbitrary unit.

Figure S7. mRNA expression of the *ICAM1, GlyCAM1, SELP,* and *SELE* genes in the skin tissue of healthy controls and SSc patients.

Skin sections from diffuse cutaneous systemic sclerosis (dcSSc) patients with disease duration of ≤1 year, dcSSc patients with disease duration of >1 year, and healthy controls were assessed (n = 4-6). Values are the means ± SEM. *$P < 0.05$. AU, arbitrary

unit.

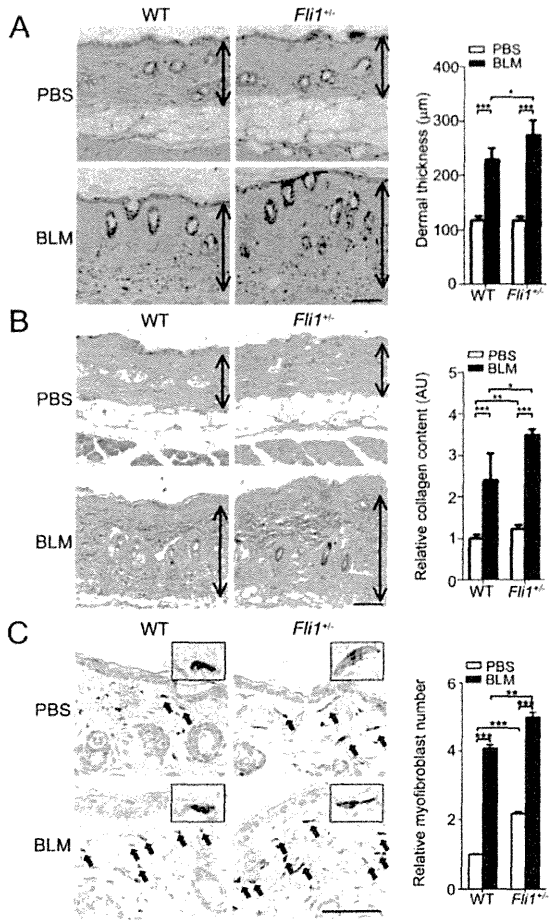

119x169mm (300 x 300 DPI)

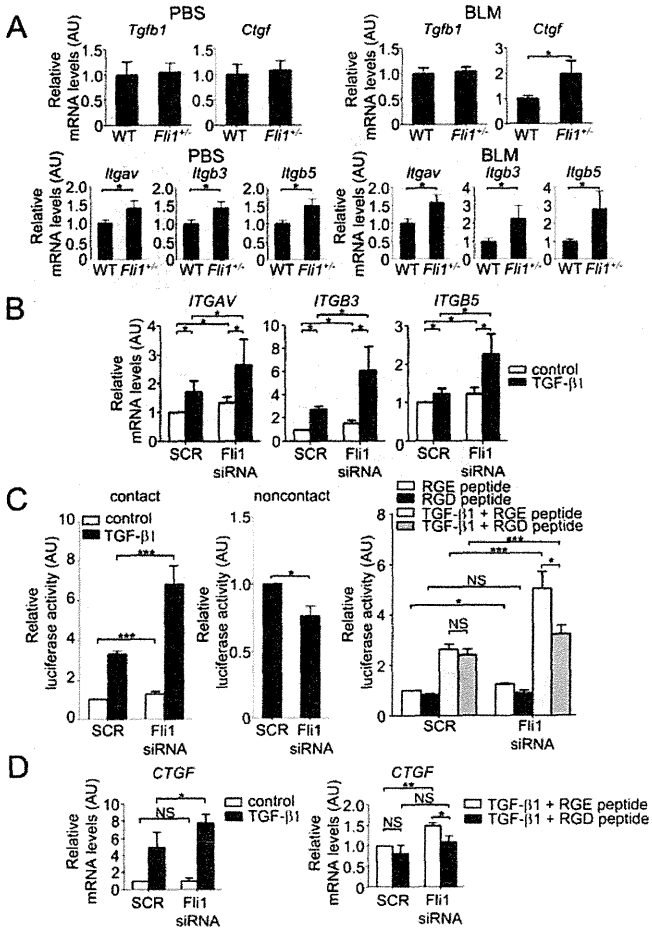

119x169mm (300 x 300 DPI)

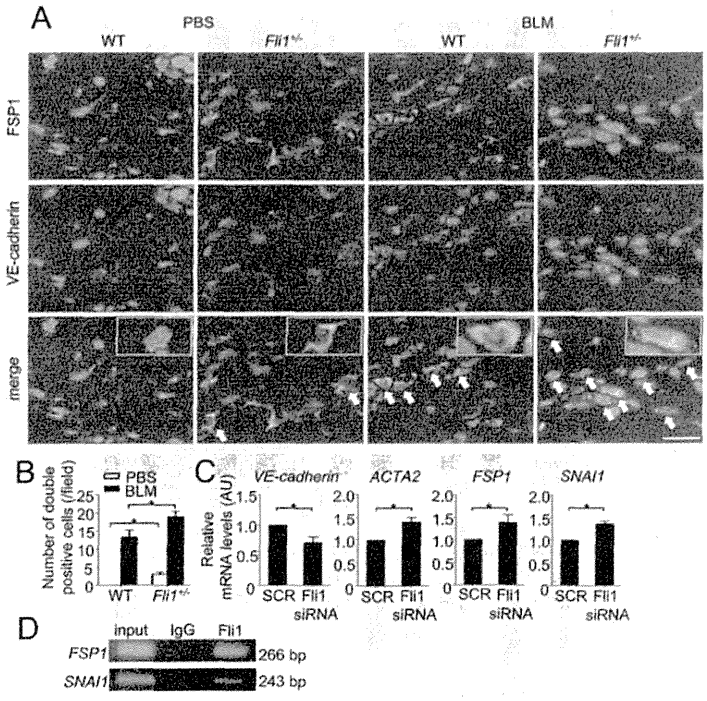

119x169mm (300 x 300 DPI)

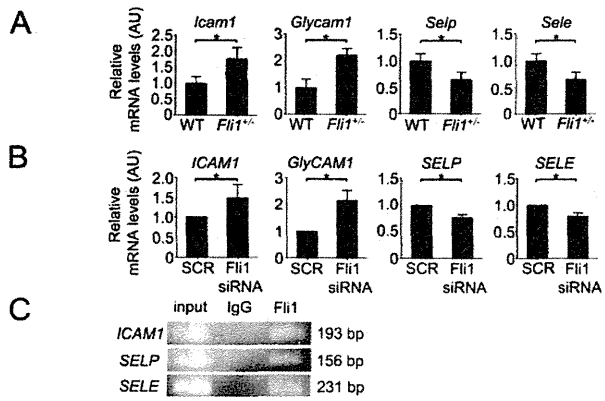

119x169mm (300 x 300 DPI)